



Payton, O., Picco, L., & al., E. (2020). Euler–Bernoulli theory accurately predicts atomic force microscope cantilever shape during non-equilibrium snap-to-contact motion. *Nanotechnology*, 31(18). <https://doi.org/10.1088/1361-6528/ab6dff>

Peer reviewed version

Link to published version (if available):  
[10.1088/1361-6528/ab6dff](https://doi.org/10.1088/1361-6528/ab6dff)

[Link to publication record in Explore Bristol Research](#)  
PDF-document

This is the author accepted manuscript (AAM). The final published version (version of record) is available online via IOP Publishing at <https://iopscience.iop.org/article/10.1088/1361-6528/ab6dff> . Please refer to any applicable terms of use of the publisher.

## University of Bristol - Explore Bristol Research

### General rights

This document is made available in accordance with publisher policies. Please cite only the published version using the reference above. Full terms of use are available: <http://www.bristol.ac.uk/red/research-policy/pure/user-guides/ebr-terms/>

1           **EULER-BERNOULLI THEORY ACCURATELY PREDICTS ATOMIC FORCE**  
2           **MICROSCOPE CANTILEVER SHAPE DURING NON-EQUILIBRIUM SNAP-TO-**  
3           **CONTACT MOTION**

4  
5           **Steven J. Eppell,<sup>1,§</sup> David Friedenber<sup>2</sup>, Oliver Payton,<sup>3</sup> Loren Picco,<sup>4</sup> Fredy R. Zypman,<sup>2,§</sup>**

6           <sup>1</sup>Biomedical Engineering Dept., Case Western Reserve University, 10900 Euclid Ave.,  
7           Cleveland, Ohio, 44122 USA  
8           sje@case.edu

9  
10          <sup>2</sup>Physics Dept., Yeshiva University, 2495 Amsterdam Ave., Manhattan, New York, 10033 USA  
11          zypman@yu.edu, dfriede1@mail.yu.edu

12  
13          <sup>3</sup>Interface Analysis Centre, H. H. Wills Physics Laboratory, University of Bristol, Bristol, UK  
14          op4664@bris.ac.uk

15  
16          <sup>4</sup>Physics Dept., Virginia Commonwealth University, Richmond, VA, 23284 USA  
17          lpicco@vcu.edu

18  
19  
20  
21  
22                           §Corresponding authors sje@case.edu, zypman@yu.edu

23

24 **ABSTRACT**

25  
26 We prove that the Euler-Bernoulli elastic beam theory can be reliably used to describe the  
27 dynamics of an atomic force microscope cantilever during the far from equilibrium snap-to-  
28 contact event. In conventional atomic force microscope operation, force-separation curves are  
29 obtained by post-processing voltage versus time traces produced by measuring one point on the  
30 cantilever close to the hanging end. In this article, we assess the validity of the Euler-Bernoulli  
31 equation during the snap-to-contact event. The assessment is based on a direct comparison  
32 between experiment and theory. The experiment uses Doppler vibrometry to measure  
33 displacement versus time for many points along the long axis of the cantilever. The theoretical  
34 algorithm is based on a solution of the Euler-Bernoulli equation to obtain the full shape of the  
35 cantilever as a function of time. The algorithm uses as boundary conditions, experimentally  
36 obtained information only near the hanging end of the cantilever. The solution is obtained in a  
37 manner that takes into account non-equilibrium motion. Within experimental error, the theory  
38 agrees with experiment indicating that the Euler-Bernoulli theory is appropriate to predict the  
39 cantilever kinematics during snap-to-contact. Since forces on the tip can be obtained from the  
40 instantaneous shape of the cantilever, this work should allow for computation of tip-sample  
41 forces during the snap-to-contact event from a conventional force-distance measured input.

42  
43 Key Words: AFM, atomic force microscopy, far from equilibrium AFM cantilever, force  
44 distance curve  
45  
46

47 **INTRODUCTION**

48  
49 The central hypothesis of this paper is that the Euler-Bernoulli equation provides a valid  
50 model by which the kinematics of an AFM cantilever can be obtained during the far-from-  
51 equilibrium snap-to-contact event. This event is often purposely avoided to stay within the  
52 regime in which harmonic analysis can be performed. However, the snap-to-contact presents a  
53 unique opportunity to test samples at closest approach. It allows for optimal sensitivity to  
54 rapidly changing surface forces, allows for optimal lateral resolution because the situation can be  
55 analyzed at arbitrarily small tip-sample separation, and provides a method for obtaining these  
56 results with a simple experimental setup that requires no lock-in amplifiers. Motivated by these  
57 observations, we sought to determine if a conventional AFM that provides cantilever  
58 displacement measures only at the hanging end, can be used in conjunction with the Euler-  
59 Bernoulli equation to obtain the full cantilever kinematics. Since forces on the tip can be  
60 obtained from the instantaneous shape of the cantilever,[1] this work should allow for  
61 computation of tip-sample forces during the snap-to-contact event from a conventional force-  
62 distance measured input.

63 Atomic force microscopy is capable of generating topographical and surface  
64 spectroscopic information even at length scales below a nanometer. To obtain this information  
65 reliably and quantitatively, it is necessary for the user to know what forces the cantilever  
66 experiences at each instant of operation. Thus, the mathematical prediction of the kinematics of  
67 the cantilever sensor plays a central role in defining the output accuracy of the force  
68 reconstruction algorithm in atomic force microscopy. To date, this description is well tested for  
69 quasi-static operation and for operation where the cantilever is driven in one or more of its  
70 normal modes. In this article, we study the validity of the assumption that the cantilever's  
71 kinematics can be obtained from the Euler-Bernoulli equation [2-4] even under the specific  
72 conditions of non-equilibrium motion and non-linear external forces. These common  
73 circumstances exist during the snap-to-contact event, when the atomic force microscope tip  
74 experiences the last few nanometers of travel before impacting the surface.

75 While the non-equilibrium motion mentioned above is not present in multifrequency  
76 operation,[5, 6] the newer commercially available techniques involving off-resonance motion of  
77 the lever as accomplished with peak force mode and fast force mapping do contain non-  
78 equilibrium motion[7]. These methods take the lever through a single stroke similar to the slow  
79 force-separation curve dealt with in the present paper.

80 In the past three decades, atomic force microscopy[8] has produced images of soft and  
81 hard matter surfaces with submicron, even nanometer resolution [9-18]. Nevertheless,  
82 considering its recent centrality in the imaging of materials surfaces and the vast technical  
83 improvements regarding data collection speed and resolution, [5, 19] the technique is not yet  
84 completely quantitative. This is due to a large extent both to the lack of full information of the  
85 interaction forces between the sample and the tip, and to an unavoidable mismatch between the  
86 mathematically modeled cantilever and the real one.

87 Since the inception of atomic force microscopy, imaging has been based on monitoring  
88 variations of experimental parameters as the cantilever/tip sensor moves from one pixel to the  
89 next. In the conventional experimental implementation of the image reconstruction, an optic  
90 lever system is used to measure the position of the tip or, more accurately, the slope of the  
91 cantilever at the tip's position. A photodetector output voltage is rapidly recorded at each pixel  
92 while the tip moves up and down as a consequence of topographical and chemical variations on

93 the surface. Thus, by looking at all pixels within the field of view, a surface image can be  
94 rendered using some function of the photodetector voltage as the contrast quantity.

95 A fundamental question presents itself naturally; what is the physical content of the  
96 voltage in regards to the surface under study? Answering this question is tantamount to learning  
97 which tip-sample interaction forces are at play in producing a motion of the cantilever, which  
98 ultimately generates the observed voltage. To build the voltage-to-force connection, it is  
99 necessary to have a reliable mathematical model that produces the kinematics of the cantilever.  
100 This model is then used to answer several questions. How does the tip sensor move under  
101 external forces? How does that induced motion effect a photodetector voltage? How does one  
102 solve the inverse problem whereby the experimental voltage, conventionally known only from  
103 the motion at one location on the cantilever, is used to reconstruct the motion of the cantilever at  
104 all points and for all times, and in due course, the sought forces acting on it?

105 Usually, a minimalistic connection is made between forces and voltages where, via  
106 simplifying approximations, the voltage is proportional to the force at every instant. The  
107 corresponding underlying assumptions, that the cantilever's deflection at its free end is  
108 proportional to the slope there, and a one-degree-of-freedom-cantilever, are too stringent for  
109 quantitative force analysis when the system is far from equilibrium.[20] More accurate  
110 approaches include treating the cantilever as a simple harmonic oscillator[21] and even more  
111 realistically, as a true extended beam that can support spatial and temporal vibrations.[20] The  
112 Euler-Bernoulli beam theory is particularly relevant to a wide range of atomic force microscopy  
113 applications because the slim cantilever's vibrations are dominated by its flexural motions. In  
114 effect, the Euler-Bernoulli equation provides a rigorous connection between the complete shape  
115 of the cantilever and the force history required to produce that shape. Thus, if the shape of the  
116 cantilever is measured experimentally and this agrees with the shape predicted by the Euler-  
117 Bernoulli equation, this is synonymous with stating that the forces experienced by the system can  
118 be accurately recovered using the Euler-Bernoulli equation. This is the central thesis driving the  
119 work we present. The work is based on an experimental design whereby the cantilever's  
120 position-vs-time curves are measured at multiple locations, not just at one point near the hanging  
121 end.

122 Several previous studies have looked at the problem of validating the accuracy of the  
123 Euler-Bernoulli theory in predicting the behavior of real atomic force microscope cantilevers.  
124 Some of this work is reviewed below. This literature provides results that are both interesting  
125 and useful to the atomic force microscopy community. However, none of the extant studies  
126 simultaneously and directly compares experiment to theory for the cantilever under non-  
127 equilibrium conditions.

128 Payam and Fathipour[22] performed a theoretical analysis of the Euler-Bernoulli  
129 equation by means of variational analysis with the goal to incorporate practical aspects of the  
130 microscope such as tip mass and cantilever geometry. Gates and Pratt[23] used Doppler  
131 vibrometry in conjunction with Euler-Bernoulli analysis to measure the cantilever's spring  
132 constant with high accuracy. This analysis did not address either transient behavior nor the full  
133 shape of the cantilever. Payton et al.[24] tackled the problem of fast imaging whereby an  
134 unknown varying force acts on the tip due to surface topography variations. While they did  
135 measure the shape of the cantilever as a function of time, the study was restricted to eigenmodes  
136 of the combined cantilever/sample system; amplitudes of the cantilever's vibration were  
137 collected at different locations at a single frequency for times long relative to the snap-to-contact  
138 event to increase reliability. This method cannot be used in our case because the snap-to-contact

139 determines naturally and suddenly what happens to the deflection of the cantilever. Zhou, Fu  
140 and Li [25] used the Euler-Bernoulli theory to extract mechanical properties of composite  
141 materials. While they did not deal with the full shape of the cantilever, they did compare Euler-  
142 Bernoulli with finite element analysis and validated the appropriateness of Euler-Bernoulli to  
143 within three percent under dynamic equilibrium conditions. Laurent, Steinberger and Bellon [26]  
144 considered a cantilever with a spherical bead at its end. They compared the normal mode shapes  
145 of Euler-Bernoulli theory with experimentally measured ones and got agreement to within ten  
146 percent for the first four modes. While they were able to measure the shape of the cantilever at  
147 multiple points versus time, they did it for normal modes and not for the general transient case.  
148 Payam[27] studied the shift in frequencies due to the presence of an ambient liquid and used the  
149 Euler-Bernoulli equation to analyze the signal but did not consider the shape of the cantilever or  
150 transient behavior. Villanueva et al.[28] were interested in the length limits of the Euler-  
151 Bernoulli equation. They found that 20  $\mu m$  long levers, corresponding in their case to a  
152 cantilever length:width aspect ratio of about five, are short enough to make the theory deviate  
153 from experiments. Zhou, Wen and Li [29] presented a theoretical study of short cantilevers and  
154 showed how to correct the Euler-Bernoulli equation via the Timoshenko theory. Their paper did  
155 not present experimental comparison nor did it consider the shape of the cantilever or transient  
156 behavior. Wagner and Killgore[30] studied the resonant motion of a cantilever under the effect  
157 of lumped or distributed forces. No transient or experimental measurements were considered.

158 In general, the difficulty in providing a definite account of the agreement between  
159 experiment and theory resides in both. On the one hand, typical atomic force microscopes are  
160 not set up to measure rapid cantilever deflections at multiple points along the lever. Thus, the  
161 full shape of the lever necessary to determine unambiguously the forces acting on it is not  
162 available. On the other hand, the theories rely on reasonable assumptions fit to the problem of  
163 interest. Thus, for example, one may be interested in cantilever free boundary conditions at the  
164 hanging end for spring constant calibration, or harmonic excitations at the base for multi  
165 frequency studies. All articles in this field use the Euler-Bernoulli equation with adaptations  
166 pertinent to the problem at hand.

167 In this context, the present paper presents new data and analysis useful in the unsolved  
168 problem of understanding the connection between theory and experiment during the snap-to-  
169 contact event. We previously showed that the classic concave up surface potential vs separation  
170 could be extracted from this motion in air [3] and in liquid [31]. These earlier papers utilized  
171 Tikhonov regularization to solve the inverse problem imposed by only having experimental  
172 measurement of the end of the lever while solution of the problem requires knowledge of the full  
173 lever shape. This is an ill-posed inversion for cases involving fast transients, like in the snap-to-  
174 contact. We inverted the Euler-Bernoulli equation in the cantilever's shape space spanned by the  
175 normal modes under conditions of an unloaded tip. This was an intrinsically limited method  
176 since, during the snap-to-contact, the tip load quickly increases thus violating the assumption of  
177 an unloaded tip used to create the basis set. More recently, we developed what should be a more  
178 robust method for converting the voltage-vs-time trace produced by the vertical motion of the tip  
179 measured at a single cantilever location into forces, the Causal Time Domain Analysis  
180 (CTDA).[32] CTDA relies on explicit consideration of the measured nonlinear voltage-time data  
181 as a boundary condition to the Euler-Bernoulli equation. When we compared Tikhonov  
182 regularization to CTDA, we found that the two approaches did not produce the same force-  
183 separation curves.[2] An obvious next step would be to use some known surface force to  
184 determine which theory performed better. However, there is currently no well-accepted standard

185 for creating a surface force that is known within a few nanometers of tip/surface contact. Thus,  
186 we decided to test CTDA against experimentally measured cantilever shapes. The choice is  
187 based on the fact that CTDA, unlike regularization, is free of tuning parameters. That is what we  
188 present in the current article, which is organized as follows. In the Methods section, we explain  
189 how conventional AFM measurements are performed and give details of our experimental setup.  
190 Also, in the Methods section, a brief description of our theory is presented. Then, in the  
191 Experimental Results section, we present the position versus time traces at multiple points along  
192 the cantilever. In the Comparison of Theory and Experiment section, we show how the theory  
193 output, i.e. the full shape of the cantilever at all times, matches with the experiment. In the last  
194 section, we present the Conclusions.

## 195 METHODS

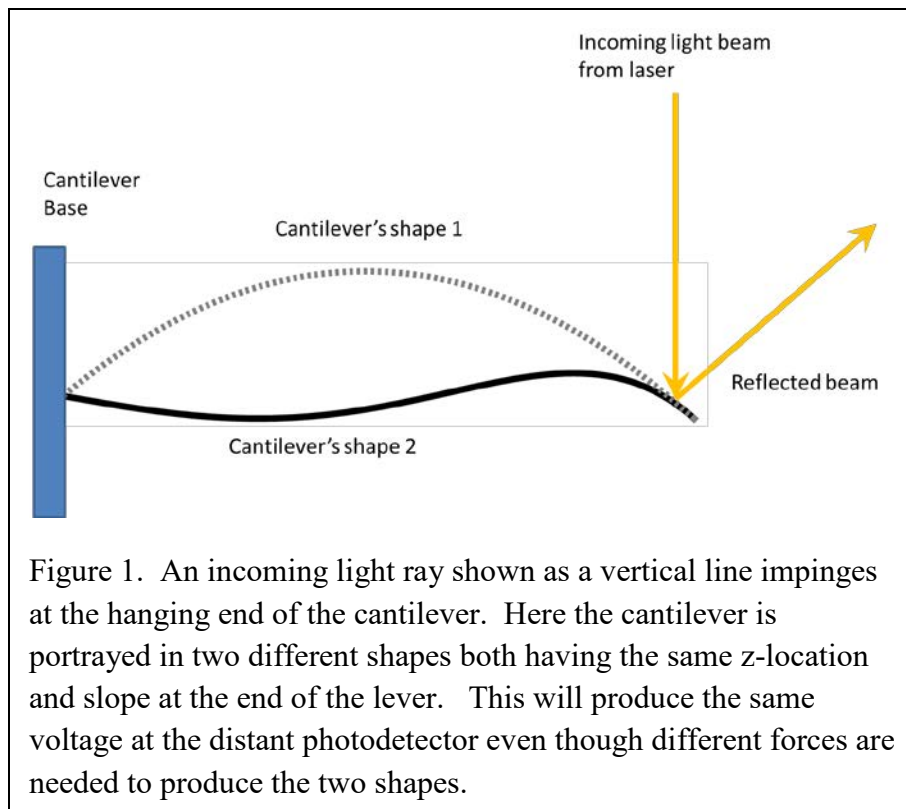
### 196 Conventional Experimental Approach

197  
200 Standard atomic force microscopes come equipped with a light detection system to  
201 measure the motion of the cantilever as shown in Figure 1. A light ray reflected off the  
202 cantilever provides a photodetector voltage that is proportional to the slope of the cantilever at  
203 the hanging end.

204 However, and as  
205 Figure 1 depicts, the  
206 instantaneous value of  
207 the slope at one point  
208 provides only partial  
209 information of the full  
210 shape of the cantilever at  
211 that instant. Since the  
212 full shape is necessary to  
213 determine the interaction  
214 force between tip and  
215 sample but is not  
216 typically available  
217 experimentally,  
218 mathematical modeling  
219 is called upon to bridge  
220 the gap between what is  
221 needed and what  
222 experiment provides.

223 One quantitative  
224 approach to make the  
225 connection relies on the  
226 Euler-Bernoulli equation

227 to predict the motion of the cantilever.[33] In one implementation using this approach[32], the  
228 instantaneous slope, proportional to the photodetector voltage, is used as a boundary condition to  
229 the Euler-Bernoulli equation. By assuming a straight cantilever as an initial condition to the  
230 problem, corresponding to a large tip-sample separation at the beginning of the experiment when



231 no interaction forces are detectable, the equation can be solved iteratively in time to obtain the  
 232 full shape of the cantilever at all future times. With this information, the interaction force at all  
 233 times is finally obtained. Afterwards, by incorporating instantaneous separation data, the sought  
 234 force-separation curve is obtained parametrically in time.

235  
 236 **Experimental Setup and Considerations**

237  
 238 The experiment is in the form of displacement versus time measurements for many points  
 239 along the long axis of the cantilever. By contrast, conventional data collection in atomic force  
 240 microscopy is at a single point, typically near the hanging end of the cantilever. Laser Doppler  
 241 vibrometry was used to monitor the motion of multiple points along the length of the cantilever  
 242 at multiple times during the snap-to-contact. A schematic of the equipment used is shown in

243 Figure 2. The method  
 244 used was similar to  
 245 that described in  
 246 Payton et al.[34]  
 247 Briefly, a vibrometer  
 248 (Polytec VIB-A-510)  
 249 was attached to a  
 250 cantilever mount at  
 251 12.5°. This allowed  
 252 for the velocity of the  
 253 cantilever in the  
 254 direction perpendicular  
 255 to the lever's surface  
 256 to be recorded with  
 257 high bandwidth (up to  
 258 20 MHz). The  
 259 substrate (a piece of  
 260 freshly cleaved mica)  
 261 was cycled  
 262 sinusoidally toward  
 263 and away from the  
 264 cantilever tip (Bruker  
 265 MSNL lever B, 200  
 266  $\mu\text{m}$  long rectangular  
 267  $\text{Si}_3\text{N}_4$  cantilever with a  
 268 spring constant of 0.02  
 269 N/m, a thermal tune

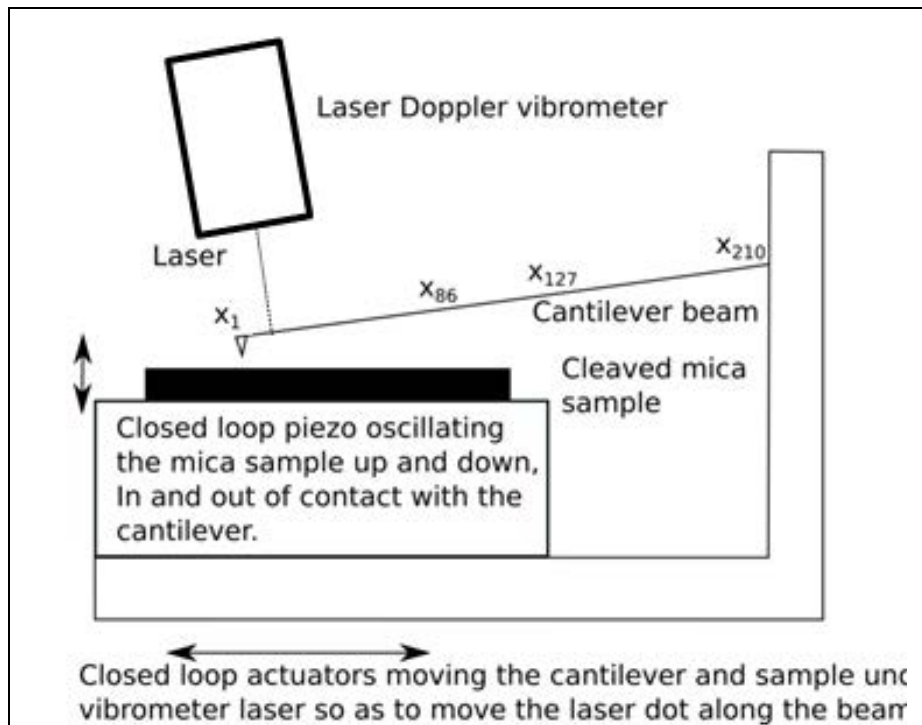


Figure 2: Diagram of the setup used to experimentally measure cantilever deflections during the snap-to-contact. The cantilever is shown with indices along the long axis of the cantilever each separated by 1  $\mu\text{m}$ .

270 measured first mode resonance of 14.65 kHz, and a pyramidal tip) using a piezo stage (Npoint  
 271 model NPXY60Z20) with closed loop capacitance control at 50 Hz with an amplitude of  
 272  $850 \pm 0.1$  nm (maximum velocity was therefore 267  $\mu\text{m/s}$ ). The data displayed was collected at  
 273 the point in the motion of the stage with the sample moving towards the cantilever tip at a  
 274 velocity of  $150 \pm 7$   $\mu\text{m/s}$ . Z-motion monitoring was done along the cantilever every 1  $\mu\text{m}$  while  
 275 the cantilever underwent multiple snaps-to-contact. To do signal averaging over several snaps at  
 276 the same point and to create an experimentally determined cantilever shape, it was necessary to



277 shift the individual snaps so they were in-phase with each other. This was done by cross-  
278 correlating the data streams over a short time period that spanned the snap-to-contact.

279 The approach velocity was taken into account when converting the difference in piezo  
280 position and cantilever deflection into tip-sample separation. Under the conditions used in our  
281 manuscript, the approach velocity was very slow compared to the cantilever velocity due to the  
282 snap-to-contact. So, there was unlikely to have been any significant modification in the situation  
283 seen by the tip due to the moving sample. The average speed of the cantilever during the snap  
284 was about 1600  $\mu\text{m/s}$ . Thus, during the 25  $\mu\text{s}$  of the snap as the tip traversed the 40 nm until  
285 contact, the stage moved by 3.8 nm. This was taken into account when producing the force-  
286 separation plots shown in the manuscript. While there was a slight drift present in the system  
287 causing the tip to snap to contact with the sample at a slightly different point in the periodic  
288 motion of the sample, this produced a sub-nanometer uncertainty in the tip-sample distance  
289 which was within the thermal noise in the system so we chose to ignore it.

290 At much higher velocities and especially in fluid, confined fluid layer effects between the  
291 cantilever and the sample surface will contribute substantially to the motion of the cantilever and  
292 will need to be taken into account when determining the tip-sample force. However, none of this  
293 is relevant to the problem of converting cantilever shape into cantilever force. In other words,  
294 these issues are important in determining tip-sample forces, but not important in determining  
295 cantilever shape.

296 Regarding non-linearity of piezo scanners, the approach was made using an Npoint stage  
297 with capacitance sensor ( $\pm 0.1$  nm). Any hysteresis in the motion of the piezos was taken into  
298 account by using the calibrated sensor values instead of the drive signal sent to the stage.

### 300 **Influence of Ambient Humidity on the measurements**

301  
302 The humidity was held constant at  $43 \pm 5\%$  RH and a  $20^\circ\text{C}$  temperature throughout the  
303 experiment. It is likely that the onset of the snap-to-contact was initiated due to thermally driven  
304 oscillations in the fluid layers on the tip and/or mica surface. The retraction of the cantilever was  
305 not the focus of the experiment therefore the formation and snapping of any meniscus was not  
306 explored. It would be expected that as the humidity increased, the size and strength of any  
307 meniscus force would increase, though this is not taken into account in the model used. Overall,  
308 these issues are of central importance in the study of the origins of tip/sample forces probed  
309 using  $F(s)$  curves but not in characterizing the kinematics of the cantilever motion. For our  
310 purposes, as long as some force, be it capillary, vDW, or electrostatic, was present that initiated a  
311 snap-to-contact, then the lever is made to move in a non-equilibrium manner as the tip snaps  
312 down to the surface.

### 314 **EXPERIMENTAL RESULTS**

315  
316 Position vs. time traces were collected as explained in the previous section. Figure 2 labels the  
317 210 positions at which time trace data were taken. We were particularly careful to gather  
318 information from bending deflections only. It is known that cantilevers tend to exhibit torsion  
319 upon snap-to-contact. The exact lateral location of the tip on the Bruker MSNL B cantilever  
320 used is not always centered on the cantilever. Therefore, the cantilever can experience a moment  
321 about the tip when the tip experiences a force such as a snap-to-contact event. The cantilever  
322 displacement was measured at points taken along a line that intersected the tip. In doing so, the

323 effect of the torsional modes are minimized in the data. Data previously collected by Payton et  
324 al.<sup>1,2</sup> using a similar method have been shown to be modelled well by a bending mode only FEA  
325 model<sup>3</sup> indicating that, with the correct placement of the points at which data is collected, the  
326 torsional modes can be ignored.

327 An example of a time trace for a single snap at a single location on the lever is shown in  
328 Figure 3. To ensure that the input to our model matched the initial conditions of the theory we  
329 used, it was necessary to have no displacement at early times corresponding to a motionless  
330 cantilever when the tip and sample are well separated and not interacting. To achieve this, we  
331 found the average displacement value prior to the snap, and then used the collected data to find  
332 the last time the recorded data achieved this value prior to entering the snap-in region. We then  
333 appended ten identical values of this average to the start of each snap thus guaranteeing a well-  
334 behaved input.

335 At some point,  
336 the tip-sample  
337 interaction becomes  
338 non-negligible and a  
339 downward trend  
340 corresponding to an  
341 attraction occurs. This  
342 is seen in Figure 3  
343 starting at around  
344  $5 \mu s$ . Eventually, the  
345 tip feels the repulsive  
346 force due to a  
347 combination of a  
348 confined fluid layer  
349 and Pauli exclusion  
350 acting on electrons in  
351 the tip and the surface.  
352 This slows the  
353 cantilever and  
354 eventually causes it to  
355 reverse direction.

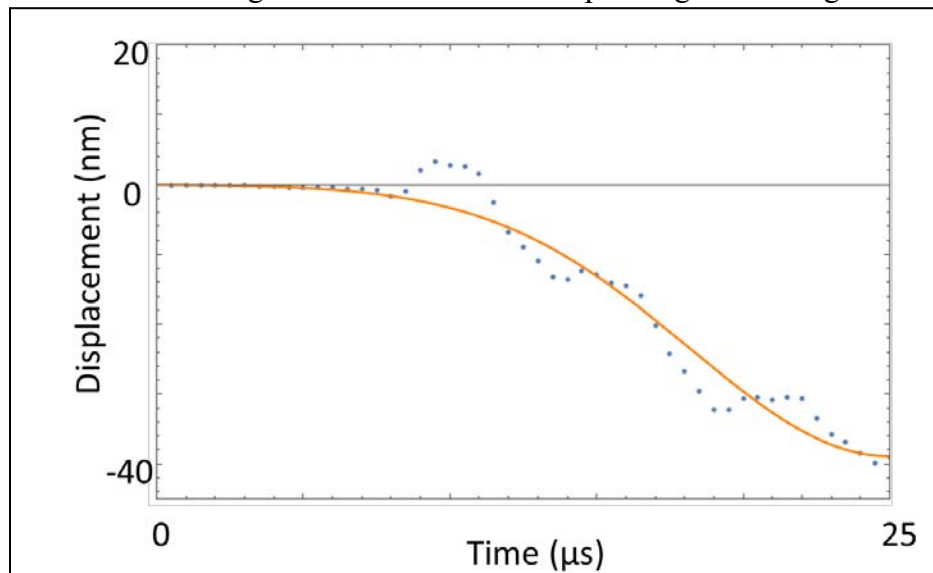


Figure 3. Snap-to-contact displacement of a point  $\sim 15 \mu m$  from the free end of the cantilever as a function of time. Also shown is a best fit EVE curve[29] that helps the eye follow the general trend and is useful in matching the phases of multiple data sets like the one shown.

356 Apparent in the typical snap-to-contact event shown in Fig. 3, are a few plateaus in the  
357 traverse of the cantilever toward the surface. In some cases, the path of the lever even seems to  
358 reverse direction for a short time before continuing on down. It is possible that high frequency  
359 oscillations of the cantilever due to the thermal bath or some other source existed as the state of  
360 the lever prior to its entering the snap-to-contact regime. It is also possible that the short time  
361 events came from some electronic source related to the Doppler system used to measure the  
362 cantilever displacements. Conventional cantilever analysis would treat these as higher order  
363 normal modes. However, the amplitude, frequency, and phase of such modes all depend  
364 intimately on the boundary conditions at the hanging end of the cantilever. During snap-to-  
365 contact, this boundary is changing so rapidly that the lever is unable to move through a complete  
366 period of an oscillation before the boundary condition has substantially changed because the tip  
367 is now closer to the surface. Thus, the concept of a mode is not well defined during the snap-to-  
368 contact event. In an attempt to determine what range of frequencies the cantilever used would go

369 through as it traversed the snap-to-contact, we solved the equations 4 and 5 in reference [33]. In  
 370 going from large separation to contact: the first free mode of the lever goes from 15 kHz to 0  
 371 kHz, the second free mode goes from 95 kHz to 75 kHz, and the third free mode goes from 266  
 372 kHz to 253 Hz. None of these ranges includes the observed oscillation frequency near 200 kHz  
 373 seen in our data. This makes it unlikely that these oscillations are a reflection of higher order

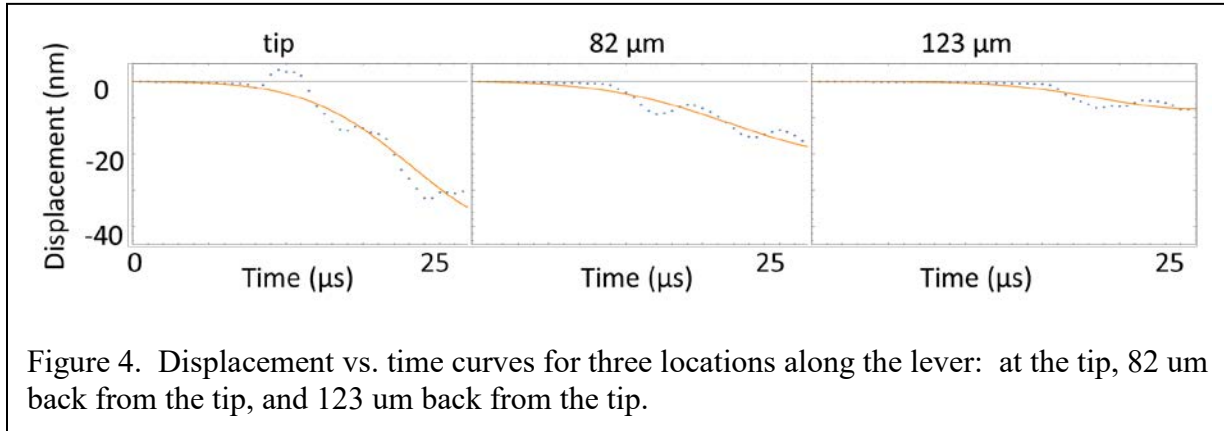


Figure 4. Displacement vs. time curves for three locations along the lever: at the tip, 82  $\mu\text{m}$  back from the tip, and 123  $\mu\text{m}$  back from the tip.

374 resonances in the lever. As an initial attempt at analyzing this complex data, we decided to focus  
 375 on the main feature of the monotonic descent of the lever toward the surface. To extract this  
 376 feature from the data, we found best-fit EVE curves[32, 35] and used these functions as inputs to  
 377 our theoretical analysis.

378 Figure 4 shows three  
 379 displacement vs time curves  
 380 corresponding to three  
 381 different locations along the  
 382 cantilever. As one looks  
 383 further away from the tip,  
 384 the onset of the snap-in gets  
 385 later in time and the  
 386 amplitude of the  
 387 displacement decreases.  
 388 The general trend is clearly  
 389 downward, however there  
 390 are a few steps in the  
 391 recorded path along the way  
 392 as described in Figure 3  
 393 above. The EVE fits are  
 394 shown as the solid lines in  
 395 each of the plots. In general,  
 396 the EVE function fit the data  
 397 very well.

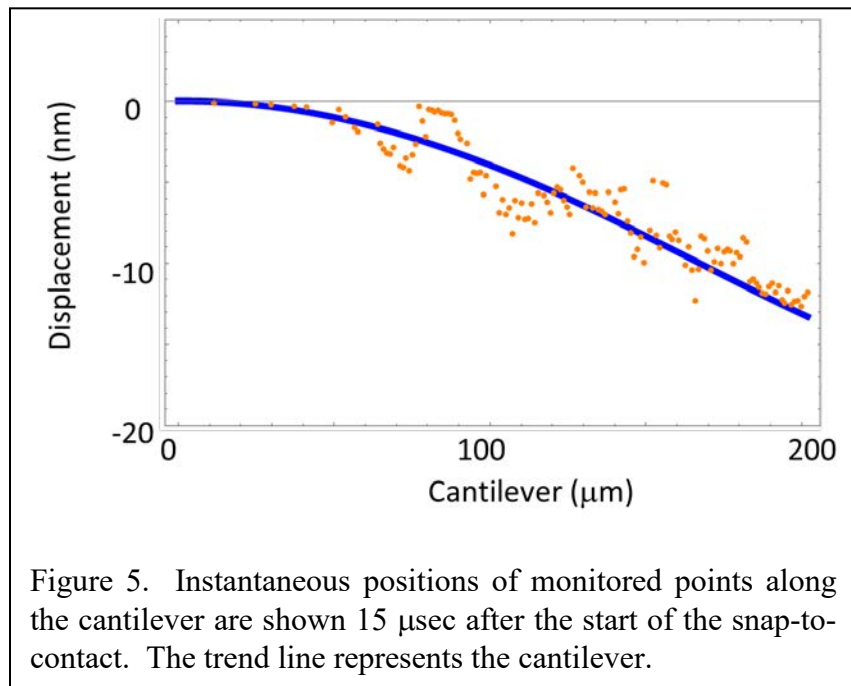


Figure 5. Instantaneous positions of monitored points along the cantilever are shown 15  $\mu\text{sec}$  after the start of the snap-to-contact. The trend line represents the cantilever.

398 A useful alternative view of the cantilever motion is given in Figure 5. There, a snapshot  
 399 of the full cantilever shape is created by plotting the position of each individual point along the  
 400 lever at one instant in time.

401  
 402

403 **COMPARISON BETWEEN THEORY AND EXPERIMENT**

404

405

406

407

408

409

410

411

412

413

414

415

416

417

418

419

420

421

422

423

424

425

426

Since the Euler-Bernoulli differential equation is 4<sup>th</sup> order in space and 2<sup>nd</sup> order in time, six constraints are needed to solve it. The constraints are obtained by setting two initial conditions and four boundary conditions. Our solution uses two initial conditions in the form of the shape of the cantilever at two consecutive early times. It is assumed that the force on the cantilever is small enough at these early times to allow for quasi-static motion. Thus, the two initial shapes are taken from unequivocally known static shapes under an external force at the free end. This effectively provides the initial shape of the cantilever and its initial state of velocities. In addition, we use two boundary conditions at the attached point namely, that the cantilever is fixed there and that it does not bend. The last two conditions are obtained by setting the vertical displacement and the slope at the hanging end of the cantilever equal to their experimentally measured values. With that input, we numerically solve the Euler-Bernoulli equation and predict the motion of all the cantilever points from the free to the fixed end. This theoretical cantilever shape vs time, relying only on measurements made near the free end of the cantilever, is then compared to the full experimentally measured motion along the whole cantilever.

To implement the solution, we took a few of the position-vs-time curves near the end of the lever and used them to determine the slope at the end of the lever. This allowed us to mimic the information available in most commercial atomic force microscopes using the direct displacement measurements provided by our Doppler technique. We emphasize that only data near the end of the lever was used to compute the entire shape of the lever. These computed shapes were then compared against the Doppler vibrometry experiments. We did this comparison in two ways. First, we looked at the displacement vs time curves for individual

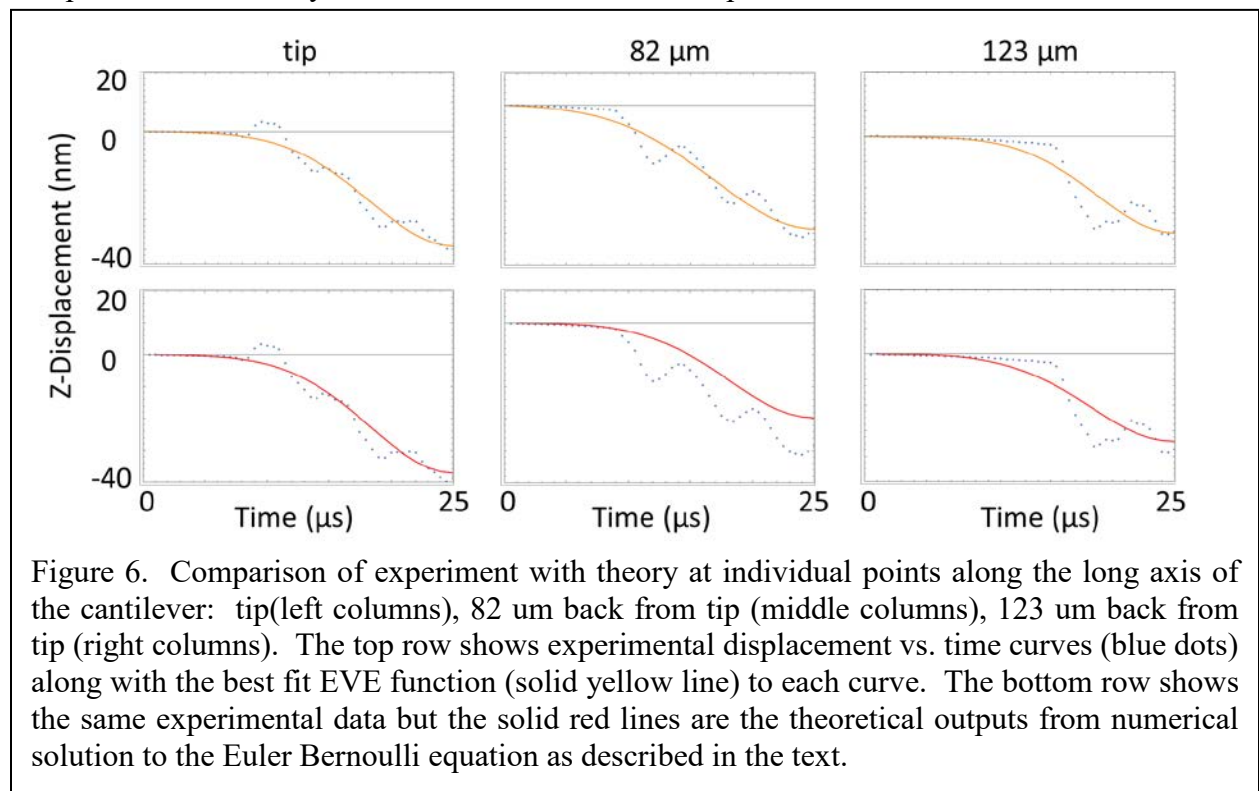


Figure 6. Comparison of experiment with theory at individual points along the long axis of the cantilever: tip(left columns), 82 μm back from tip (middle columns), 123 μm back from tip (right columns). The top row shows experimental displacement vs. time curves (blue dots) along with the best fit EVE function (solid yellow line) to each curve. The bottom row shows the same experimental data but the solid red lines are the theoretical outputs from numerical solution to the Euler Bernoulli equation as described in the text.

427 locations along the lever. Second, we looked at the entire shape of the lever at a given time  
428 point.

429 To compare theory with experiment at single points along the lever, Figure 6 shows time  
430 traces at the same three points as in Figure 4 together with the theoretical outputs. The top row  
431 of curves shows these experimentally determined plots with the EVE function best fits. The  
432 lower set of curves shows the same experimental data but the solid lines represent the output  
433 from the model which used the Euler-Bernoulli solutions using data only near the end of the  
434 lever to compute the solid curves. Experiment and theory agree well at the tip (left most plots in  
435 Fig. 7) which is expected since this is what was used as the input to the model. Experiment and  
436 theory also fit well 123  $\mu\text{m}$  back from the end of the lever. However, the fit 82  $\mu\text{m}$  back from  
437 the end is not as good. Looking carefully at noise in the system will allow us to determine if the  
438 overall motion of the cantilever is well captured by our model or not.

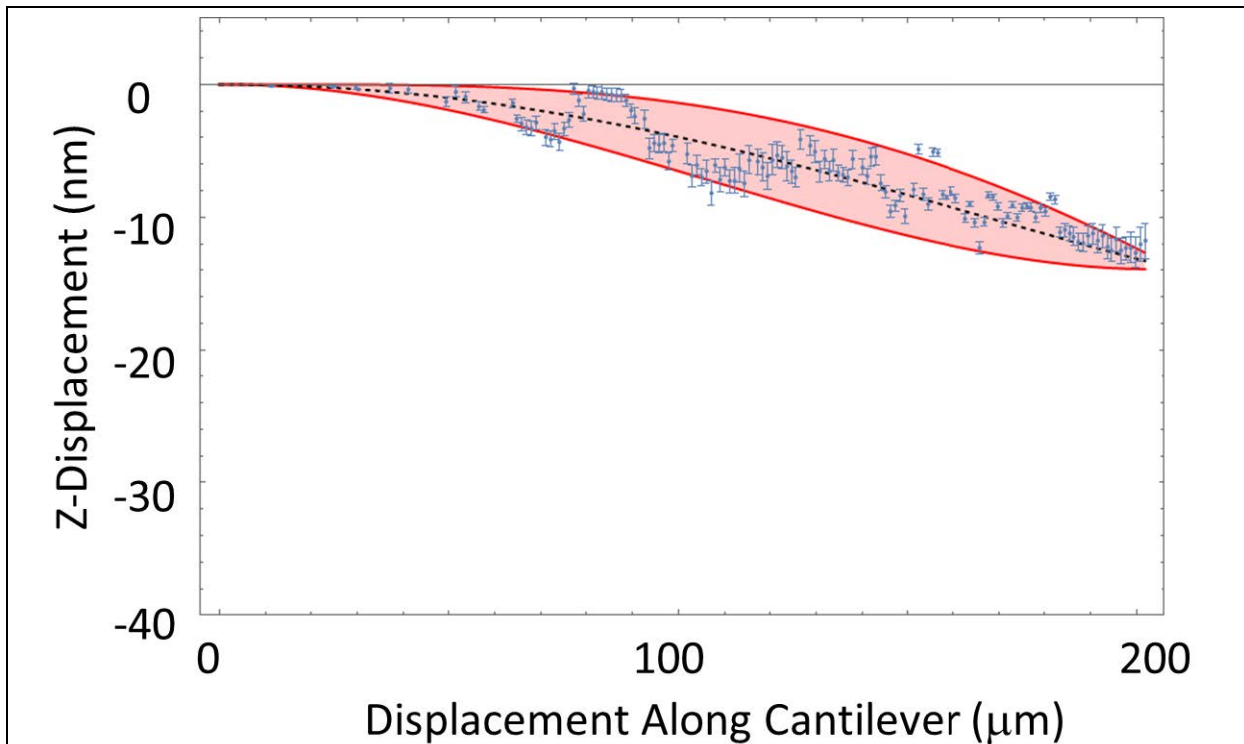
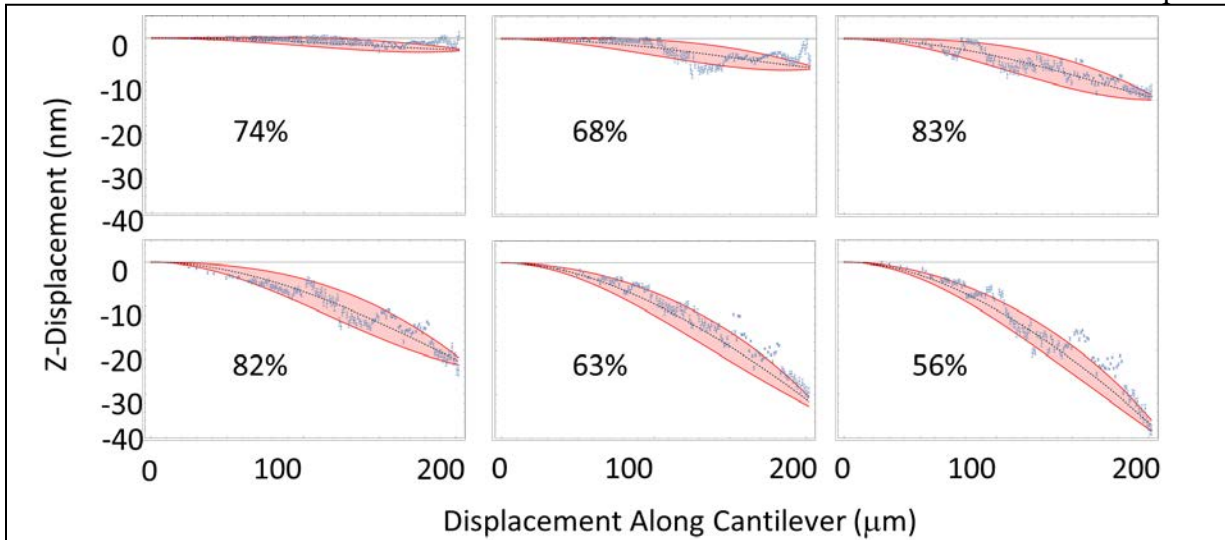


Figure 7. Snapshot of the shape of the full cantilever at an instant in time. Blue dots are the experimentally measured points. The black dotted line is the best fit to the theory. The red shaded region corresponds to the range of theoretical curves obtained using  $\pm$  one standard deviation in the experimental input error to the measured slope at the end of the cantilever.

439 Substantial measurement noise propagated from the input of our model to its output. To  
440 understand how this affected the deviation between experiment and theory, it was necessary to  
441 perform an error analysis that contained as much of the noise and its propagation through the  
442 model as possible. To this end, we used five data points near the end of the cantilever to  
443 determine its slope. In the absence of noise, any pair of these five points would have yielded the  
444 same slope. Because of the presence of noise, we obtained a population of slopes from all pair  
445 combinations and used this to compute a standard deviation of the noise. This population was  
446 used in the analysis that follows to find an envelope of model shapes of the cantilever.

447 As a second way to compare experiment with theory, a typical snapshot of the lever with  
 448 errors displayed is shown in Figure 7. The blue points with small error bars represent the  
 449 experimentally determined locations of the lever at that particular location along the long axis of  
 450 the lever. The dashed black line corresponds to the average theoretical value for the z -position  
 451 of each location along the long axis of the lever. The shaded region represents the error in the  
 452 model output based on the measured error in the input data. Specifically, five locations near the  
 453 end of the lever were used. These locations were close enough together so that they should have  
 454 all produced the same slope. In fact, they provided a range of slopes. The standard deviation of  
 455 the slope was found and then the mean plus or minus one standard deviation was used as an input  
 456 to the model. This produced a range of shapes that falls within the shaded region. Note: this  
 457 slope is used as an input at each time point in the model. Thus, a different standard deviation  
 458 and a different shaded region were computed at each time point.

459 Figure 8 shows six different snapshots of the snap-to-contact portion of the curve  
 460 displayed in the same way as Figure 7. A movie showing the whole trajectory of the whole  
 461 cantilever during the snap-to-contact corroborates what is displayed in Figure 8 (see  
 462 supplemental data). While there are some experimental points that fall outside the shaded  
 463 region, it is clear that the majority of experimental points fall within the computed error. For the  
 464 six typical snapshots shown in Figure 9, an average of 71% of the experimental points fall within  
 465 one standard deviation of the mean. Assuming a Gaussian distribution of the experimental  
 466 points about some “true mean,” the obtained distribution of experimental points about the  
 467 theoretical curves is as expected.



**Figure 8.** Superimposed experimental measurements and theoretical predictions based on the Euler-Bernoulli equation. Experimental results are shown as dots. Theory is displayed as a dashed line representing the best fit cantilever shape with a shaded region around it representing theoretical outcomes that fall within one standard deviation of the experimental means assuming normally distributed errors. Percentages reflect how many of the experimental points fall within the shaded regions around the theoretical curves.

468 This gives substantial evidence that the Euler-Bernoulli equation in general, and our  
 469 model for solving the ill-posed problem present when trying to convert the data provided by  
 470

471 most commercial atomic force microscopes into known cantilever shapes, provide correct  
472 solutions.

473

## 474 **CONCLUSIONS**

475

476 We find that the Euler-Bernoulli theory is an appropriate framework to predict the kinematics of  
477 the cantilever during the far-from-equilibrium snap-to-contact event. We show by direct  
478 comparison with Doppler vibrometry experiments the validity of the force-separation  
479 reconstruction algorithm based on the Euler-Bernoulli equation. Specifically, we did this  
480 comparison for the case of a cantilever undergoing far-from-equilibrium motion driven by non-  
481 linear forces during the snap-to-contact event. The relevance of our result is that, unlike in the  
482 experiment used here, conventional atomic force microscopy experimental conditions allow  
483 collection of the slope or position vs time at only a single point on the cantilever. While our  
484 rendering of the Euler-Bernoulli-based algorithm allows for the reconstruction of the full shape  
485 of the cantilever at all times, the reliability of these shapes rests ultimately on the validity of the  
486 model used. Our proof thus paves the way to use our reconstruction algorithm under  
487 conventional atomic force microscopy operating conditions. The time-consuming multiple  
488 Doppler vibrometry measurement, while central to our test, is shown here to be no longer needed  
489 when running conventional atomic force microscopy experiments. Indeed, once one knows that  
490 Euler Bernoulli can be used during snap-to-contact to predict the shape of the cantilever, the  
491 bending forces are readily attainable. In other words, our results should extend the ability to  
492 produce accurate force-separation curves from conventional voltage-time traces into far-from-  
493 equilibrium motion and non-linear interactions.

494

## 495 **ACKNOWLEDGMENTS**

496

497 This project is funded by the National Science Foundation Grant No. CHE-1508085, The  
498 Alexander Fund, and The Kressel Fellowship (DF).

499

500

501 REFERENCES

- 502
- 503 1. ZYPMAN F. Fast Atomic Force Microscopy. Encyclopedia of Nanoscience and  
504 Nanotechnology 2004. p. 307.
- 505 2. Eppell SJ, Liu YH, Zypman FR. Accuracy of AFM force distance curves via direct  
506 solution of the Euler-Bernoulli equation. AIP Advances. 2016;6(3).
- 507 3. Todd BA, Eppell SJ, Zypman FR. Squeezing out hidden force information from scanning  
508 force microscopes. Applied Physics Letters. 2001;79(12):1888-90.
- 509 4. Zhang JB, Xi N, Li GY, Su CM, Ieee. Atomic Force Microscopy sensing using multiple  
510 modes2006. 3928-+ p.
- 511 5. Dufrene YF, Ando T, Garcia R, Alsteens D, Martinez-Martin D, Engel A, et al. Imaging  
512 modes of atomic force microscopy for application in molecular and cell biology. Nature  
513 Nanotechnology. 2017;12(4):295-307.
- 514 6. Santos S, Lai CY, Olukan T, Chiesa M. Multifrequency AFM: from origins to  
515 convergence. Nanoscale. 2017;9(16):5038-43.
- 516 7. Xu K, Sun WH, Shao YJ, Wei FN, Zhang XX, Wang W, et al. Recent development of  
517 PeakForce Tapping mode atomic force microscopy and its applications on nanoscience.  
518 Nanotechnol Rev. 2018;7(6):605-21.
- 519 8. Voigtländer B. Scanning probe microscopy. Berlin: Springer; 2015.
- 520 9. Chen L, Wen JL, Zhang P, Yu BJ, Chen C, Ma TB, et al. Nanomanufacturing of silicon  
521 surface with a single atomic layer precision via mechanochemical reactions. Nature  
522 Communications. 2018;9.
- 523 10. de Pablo PJ. Atomic force microscopy of virus shells. Seminars in Cell & Developmental  
524 Biology. 2018;73:199-208.
- 525 11. Gao Y, Wang JK, Zhong J, Wang YL, Yin QX, Hou BH, et al. Application of Atomic  
526 Force Microscopy in Understanding Crystallization Process. Science of Advanced Materials.  
527 2017;9(1):89-101.
- 528 12. Hussain D, Ahmad K, Song JM, Xie H. Advances in the atomic force microscopy for  
529 critical dimension metrology. Measurement Science and Technology. 2017;28(1).
- 530 13. Li M, Dang D, Xi N, Wang YC, Liu LQ. Nanoscale imaging and force probing of  
531 biomolecular systems using atomic force microscopy: from single molecules to living cells.  
532 Nanoscale. 2017;9(45):17643-66.
- 533 14. Li M, Xi N, Wang YC, Liu LQ. Applications of Multiparametric Imaging Atomic Force  
534 Microscopy in Probing Cellular and Molecular Mechanics. Progress in Biochemistry and  
535 Biophysics. 2018;45(11):1106-14.
- 536 15. Ruggeri FS, Sneideris T, Vendruscolo M, Knowles TPJ. Atomic force microscopy for  
537 single molecule characterisation of protein aggregation. Archives of Biochemistry and  
538 Biophysics. 2019;664:134-48.
- 539 16. Setvin M, Wagner M, Schmid M, Parkinson GS, Diebold U. Surface point defects on  
540 bulk oxides: atomically-resolved scanning probe microscopy. Chemical Society Reviews.  
541 2017;46(7):1772-84.
- 542 17. Sharma S, LeClaire M, Gimzewski JK. Ascent of atomic force microscopy as a  
543 nanoanalytical tool for exosomes and other extracellular vesicles. Nanotechnology. 2018;29(13).
- 544 18. Zhong J, Yan J. Seeing is believing: atomic force microscopy imaging for nanomaterial  
545 research. Rsc Advances. 2016;6(2):1103-21.



- 546 19. Pavlicek N, Gross L. Generation, manipulation and characterization of molecules by  
547 atomic force microscopy. *Nature Reviews Chemistry*. 2017;1(1).
- 548 20. Todd BA, Eppell SJ, Zypman FR. Improved analysis of the time domain response of  
549 scanning force microscope cantilevers. *Journal of Applied Physics*. 2000;88(12):7321-7.
- 550 21. Schroeter K, Petzold A, Henze T, Thurn-Albrecht T. Quantitative Analysis of Scanning  
551 Force Microscopy Data Using Harmonic Models. *Macromolecules*. 2009;42(4):1114-24.
- 552 22. Payam AF, Fathipour M. Modeling And Dynamic Analysis Of Atomic Force Microscope  
553 Based On Euler-Bernoulli Beam Theory. *Digest Journal of Nanomaterials and Biostructures*.  
554 2009;4(3):565-78.
- 555 23. Gates RS, Pratt JR. Accurate and precise calibration of AFM cantilever spring constants  
556 using laser Doppler vibrometry. *Nanotechnology*. 2012;23(37).
- 557 24. Payton OD, Picco L, Miles MJ, Homer ME, Champneys AR. Modelling oscillatory  
558 flexure modes of an atomic force microscope cantilever in contact mode whilst imaging at high  
559 speed. *Nanotechnology*. 2012;23(26).
- 560 25. Zhou XL, Fu J, Li FX. Contact resonance force microscopy for nanomechanical  
561 characterization: Accuracy and sensitivity. *Journal of Applied Physics*. 2013;114(6).
- 562 26. Laurent J, Steinberger A, Bellon L. Functionalized AFM probes for force spectroscopy:  
563 eigenmode shapes and stiffness calibration through thermal noise measurements.  
564 *Nanotechnology*. 2013;24(22).
- 565 27. Payam AF. Sensitivity of flexural vibration mode of the rectangular atomic force  
566 microscope micro cantilevers in liquid to the surface stiffness variations. *Ultramicroscopy*.  
567 2013;135:84-8.
- 568 28. Villanueva LG, Karabalin RB, Matheny MH, Chi D, Sader JE, Roukes ML. Nonlinearity  
569 in nanomechanical cantilevers. *Physical Review B*. 2013;87(2).
- 570 29. Zhou XL, Wen PF, Li FX. Vibration analysis of atomic force microscope cantilevers in  
571 contact resonance force microscopy using Timoshenko beam model. *Acta Mechanica Solida  
572 Sinica*. 2017;30(5):520-30.
- 573 30. Wagner R, Killgore J. Reconstructing the distributed force on an atomic force microscope  
574 cantilever. *Nanotechnology*. 2017;28(10).
- 575 31. Todd BA, Eppell SJ. Probing the limits of the Derjaguin approximation with scanning  
576 force microscopy. *Langmuir*. 2004;20(12):4892-7.
- 577 32. Mehlman J, Zypman FR. Scanning Probe Microscope Force Reconstruction Algorithm  
578 via Time-Domain Analysis of Cantilever Bending Motion. *Journal of Advanced Microscopy  
579 Research*. 2014;9(3):268-74.
- 580 33. Zypman FR, Eppell SJ. Analysis of scanning force microscope force-distance data  
581 beyond the Hookian approximation. *Journal of Vacuum Science & Technology B*.  
582 1998;16(4):2099-101.
- 583 34. Payton OD, Picco L, Champneys AR, Homer ME, Miles MJ, Raman A. Experimental  
584 observation of contact mode cantilever dynamics with nanosecond resolution. *Review of  
585 Scientific Instruments*. 2011;82(4):5.
- 586 35. Eppell SJ, Feinstein M, Li L, White B, Zypman FR. Signal distortion in atomic force  
587 microscopy photodetector. *Review of Scientific Instruments*. 2017;88(10).

588